JOURNAL OF MATERIALS SCIENCE 29 (1994) 1011–1024

Mechanical properties and microstructure of a P/M aluminium matrix composite with δ-alumina fibres and their relation to extrusion

J.H. TER HAAR, J. DUSZCZYK
Laboratory of Materials science, Delft University of Technology, Rotterdamseweg 137, 2628 AL, Delft, The Netherlands

Saffil short fibre-reinforced aluminium composites have been prepared via a powder metallurgy route. Three different reduction ratios of extrusion were investigated. The tensile mechanical properties at room and elevated temperature and the microstructure, with emphasis on fibre length, were evaluated. The reduction ratio did not influence mean fibre length, implying that during the extrusion the main fibre breakage occurred in the initial compaction stage. The relative strengthening of the unidirectionally reinforced composites at room temperature is low and depends on extrusion reduction ratio. At elevated temperature the strength of the composites in the longitudinal direction is significantly higher compared to that of the base alloy. At 250 °C, improvements were obtained of 15%, 24% and 43% for V_f = 0.048, 0.100 and 0.200, respectively. It is suggested that strengthening is possible by the combined effect of a high ductility of the matrix and the resistance to plastic flow exerted by dislocations and stress fields around aligned fibres. All composites contain highly fibre-enriched layers, with bad internal cohesion. They originate from fibre clusters and form severe macroscopic defects during machining operations. Despite that, the tensile properties in the longitudinal direction are reasonably good.

1. Introduction

The production and processing of discontinuous fibre-reinforced aluminium composites are productive research subjects [1–6] having technological as well as scientific importance. The most common methods of production may be classified as liquid metallurgy (L/M) or powder metallurgy (P/M).

In the L/M technique of squeeze casting, fibre-preforms are infiltrated with the liquid metal, producing nearly fully dense composites with pseudo-three-dimensionally random fibre orientation. Good properties were achieved with this method [1]. Extrusion may be subsequently applied to fibre-reinforced cast billets [3] to obtain a finer microstructure and alignment of fibres, in order to improve the effectivity of the fibre reinforcement. The high shear stresses inherent in solid state processing may lead to extensive fibre breakage [3–6]. This is a major problem during composite production by conventional powder processing (including extrusion). However, this P/M production method directly yields unidirectional fibre-reinforced composites with a fine matrix microstructure, and further combines advantages such as flexibility of alloy chemistry and lower reactivity due to sub-solidus consolidation.

The present study is concerned with the evaluation of the mechanical properties and microstructure of such a unidirectionally aligned fibre-reinforced composite produced by a conventional powder metallurgy route and extrusion. The influence of the reduction ratio of extrusion was investigated. The latter was considered to be an important variable with regard to fibre length and matrix microstructure.

2. Experimental procedure

2.1. Materials and motivation

Relevant data on the base materials are given in Table I. The aluminium powder was produced by air atomization giving rise to cooling rates in the range 10^4–10^6 °C s^{-1}. Owing to this method of production, the particles possess an oxide surface layer of a thickness in the order of 10 nm [7]. The particles are rounded and of irregular shape. The size distribution is wide and asymmetric, with a geometrical mean of 26 μm. In this work the particle size, including that of aluminium oxide fibres, is defined as the maximum chord length in optical microscopic view.

The hypereutectic Al–Si alloy is used by the automotive industry, among others, in engine parts. It has an attractive combination of properties such as a high thermal conductivity, high wear resistance, relatively low thermal expansion and good strength at room temperature (RT); the ductility, however, is low. It has

0022–2461

inherited these, mostly favourable, properties mainly from the rapid solidification processing of air atomization, giving the powder its fine microstructure. After extrusion, the microstructure coarsens to some extent, but still leaving sizes of the order of one to a few micrometers for the matrix grains and silicon particles, respectively. The silicon phase is strong, relatively stiff and brittle under all processing conditions. The alloy may thus be regarded as a metal matrix composite having a near 20 vol % silicon particle reinforcement. Its fracture behaviour is largely determined by this silicon-phase. From a microstructural and fractographic study, Zhou and Duszczyk [8] suggested that at room temperature, the alloy fails prematurely in a brittle manner involving the cracking of primary silicon particles and decohesion between eutectic silicon crystals and the matrix. At 300 °C, failure was reported to occur by ductile microvoid nucleation, growth and coalescence at the interface between silicon crystals and the matrix. It was also previously found that at temperatures above 200 °C, the T6 heat-treatment normally applied to this heat-treatable alloy becomes superfluous because it yields worse results than the as-extruded condition [9]. By introducing a ceramic reinforcement, some improvements in tensile properties at these conditions were pursued. Because most benefit can be obtained with fibrous reinforcement, and because economical aspects were also taken into account, the use of the Saffil δ-Al_2O_3 fibre was explored.

The Saffil fibre (type RF590) has an average diameter of 3 μm and a starting length of ~ 200 μm. In the as-received stage the fibres form clusters with a size varying from 0.5–5 mm. It is fabricated by a sol–gel process and consists mainly of the δ-alumina crystallographic modification. This is a so-called transition alumina which is stabilized by the addition of 4% SiO_2. With respect to the bulk, the surface of the fibre is enriched with SiO_2. The Saffil alumina fibre has a relatively low concentration of trace elements [10]. The presently acquired material, which was milled by the manufacturer for sizing purposes, possesses ample open porosity, resulting in a high value of specific surface area (Table I). The fibres were also found to contain a large quantity of water [11], condensed at and adsorbed to the internal surface.

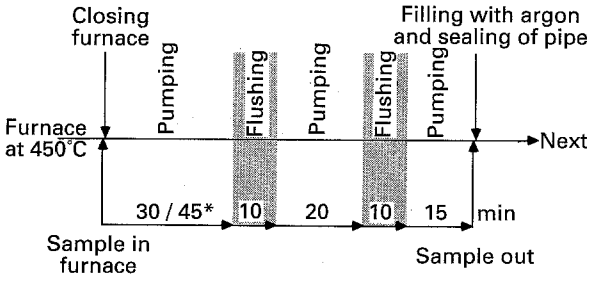

Figure 1 Outline of applied degassing procedure. (*) Holding time for composites.

2.2. Composite fabrication

The composites were prepared by dry mixing the aluminium powder and Saffil fibres in a ball mill [12]. Mass fractions of fibres, M_f, of 0.059, 0.121 and 0.237 were applied, aiming at nominal volumetric fibre fractions, V_f, of 0.048, 0.100 and 0.200 (using 3.3 $\times 10^3$ kg m^{-3} for the fibre density). Where, in the next part of this paper, V_f and M_f are used, they should be interpreted as the nominal parameters. Compaction of 300–350 g powder was performed in aluminium cans up to 60% full density. The pressures applied during this cold deformation were deliberately kept low to restrict fibre breakage at this stage. After sealing the cans by welding, vacuum degassing alternating with argon flushing was applied at 450 °C (Fig. 1). The vacuum (down to 0.1 Pa) was established with a rotary pump. Flushing with argon of at least 99.998% purity was done at 0.19 MPa. Each degassing was terminated with the admittance of argon at 0.19 MPa and squeezing of the soft aluminium tube while still hot. The cans were left to cool in the air.

Extrusion was performed at 450 °C after heating from ambient temperature in 2 h and subsequent soaking times of 0.5–1.25 h. Flat dies were used, giving extrusion reduction ratios of 10:1, 18:1 and 38:1. The maximum extrusion pressure was the same for all materials (1050 MPa). The extrudates were round bars of diameter 16.0, 12.1 and 8.5 mm, respectively.

2.3. Materials evaluation

Chemical analyses were performed on the material extruded at 18:1, to check for possible metallic contaminations and to verify the fibre contents in the extrudates. The oxide mass fractions were obtained

TABLE I Relevant data on the base materials used in this study.

	Tradename	
	ASCM20[a]	Saffil Milled RF590[b]
Composition (wt%)	20 Si–3Cu–1 Mg–0.3 Fe	96–97 Al_2O_3/3–4 SiO_2
Production method	Air-atomization	Solution spinning
Mean particle/fibre size	26 μm	200 μm
Specific surface area (10^3 m^2 kg^{-1})	0.19	16.8
Density (10^3 kg m^{-3})	2.67	3.3/3.0
Macroscopic appearance	Free-flowing powder	Granular wadding

[a] Trademark of Showa Denko K.K., Japan.
[b] Trademark of ICI, Runcorn, UK.

gravimetrically after dissolution of the matrix with NaOH and HCl solutions. Bulk chemistry of the material was analysed with inductively coupled plasma–optical emission spectroscopy (ICP–OES) as well as with X-ray fluorescence (XRF). In the case of ICP–OES, the materials were dissolved in a mixture of nitric acid and fluoric acid, after which boric acid was added to bond silicon.

The density of the extruded materials was measured by a method based on Archimedes' principle.

The hydrogen contents of the materials were measured by argon carrier gas extraction in the solid state to check for a possible effect on mechanical properties. The analysis of hydrogen in solid aluminium is rather controversial in the literature. This is because solubility and diffusivity may be substantially influenced by microstructure [13] and alloy impurity level [14]. Thus, hydrogen values in absolute terms are of little significance, especially when details of chemistry and processing are concealed. However, for comparative purposes within one body of research, these data may provide valuable information, such as, for example, directives for processing.

The measurements were performed with a Ströhlein H-mat 251 gas analyser. The apparatus has a measuring sensitivity of 0.001 p.p.m., a measuring range of up to 80 p.p.m. for a sample weight of 2 g, and an accuracy of $\pm$ 0.05 p.p.m. or 2% hydrogen content [15]. Samples were dry-machined from grip sections of RT-tested tensile specimens which, in their turn, were machined with methylated spirit (for surface smoothness). After weighing, a sample of 1.5–2 g were transferred to the furnace at 550 °C in a quartz boat. The furnace zone was continuously flushed with argon so that air was not allowed to enter. Hydrogen evolved from the sample was transported with the argon carrier gas and was measured as a change in conductivity of the gas mixture. The detector was calibrated prior to the analysis with the signal of a known volume of hydrogen. The hydrogen content of a sample was obtained by integration of the signal over a period of 20 min. A recorder was installed to record the signal of detected hydrogen against time.

Round tensile test samples were machined from the extruded bars following three designs; design D1 for use at room temperature, having a length of 74 mm and a gauge length to diameter of 36/6 mm; design D2 with shoulder sections for material extruded at an extrusion ratio of 38:1 and for tests at elevated temperature, with length of 74 mm and a gauge length to diameter of 36/4 mm; design D3, like D2, except for the gauge length to diameter being 36/6 mm for material with the other reduction ratios and tests at elevated temperature.

The tensile properties of the materials at all extrusion ratios (ER) were determined at room temperature (RT) and 250 °C. For materials with an ER of 18:1 tensile properties were also measured at 350 °C. Despite heat treatability of the matrix, no heat treatment was applied in the present case. A separate study as the effect of heat treatment of these composites on mechanical properties [16] proved that the T6 temper indeed performed worse at high temperature (250 °C) than the asextruded. For the tests at 250 and 350 °C, a Quad E4-10 three-element radiant heating chamber was employed. Prior to testing, the samples were annealed for 100 h at the test temperature and water quenched. The strain-rate applied was $1.67 \times 10^{-4} s^{-1}$. During RT tests, a 10 mm extensometer was installed, enabling the measurement of elastic modulus.

During extrusion of a fibre-reinforced composite, fibres tend to align in the extrusion direction. The length and distribution of fibres may affect the mechanical properties of the composite. Therefore, fibres are an important microstructural element. Their lengths after extrusion were determined at each ER by optical microscopy using two different sample preparation methods; (a) metallographic sectioning (Method A) and (b) separation of fibres through matrix dissolution (Method B). In the first technique, fibres were imaged in polished sections parallel to the extrusion axis (longitudinal). In the second technique, fibres were extracted from the metal matrix. The matrix was dissolved in KOH, after which the fibres were decanted, rinsed in distilled water and ethanol, and redispersed in a solution of 2% collodion in butylacetate. A drop of this suspension quickly transferred to the clean surface of a glass slide, spreads out and immobilizes the dispersed particles in the drying transparent collodion (modified after a procedure from Orr and Dallevalle mentioned elsewhere [17]).

Fibres in the samples thus obtained are detected and measured by means of semiautomated image analysis. The system used was a Leitz CBA 8000 in conjunction with a Zeiss Jenavert microscope and a CCD colour camera. Count-weighted distributions of fibres were obtained. One problem in the imaging of fibres in samples of Method A was the transparency of the fibres, causing internal reflections. The latter resulted in irregular grey levels and varying contrast with the matrix, preventing accurate detection of the fibres by the software. The problem was solved with a technique of interference etching, in which a homogeneous film of ZnTe with a high refractive index was deposited on a specimen surface. By applying monochromatic light and a specific film thickness, a reflectivity minimum is obtained for the aluminium matrix. This condition is not met at the surface of the ceramic fibres: a different phase shift during reflection makes them appear brighter and smoother. Single fibres in samples obtained with Method B could be easily imaged and detected in transmitted light microscopy by using a reflecting background.

The method of *in situ* measurement of the length of fibres in the composites (Method A) is based on the assumption that the fibres are perfectly aligned in the extrusion direction. However, this is certainly an oversimplification, and some form of a distribution of orientations around a mean will occur. For measurement of fibrelength in the powders at stages after mixing and compaction, the much more time consuming Method B preparation was necessarily used. In the present work, a comparison will be made between fibre sizes in an extruded composite obtained with both sampling methods.

TABLE II Composition by gravimetrical analysis and ICP–OES of materials extruded with reduction ratio of 18:1

V_f (vol%)	Composition (wt%)									
	M_f	M_{ox}^a	[Si]	[Si][b]	[Cu]	[Cu][b]	[Mg]	[Mg][b]	[Fe]	[Fe][b]
powder	–	–	20.0	–	3.1	–	0.63	–	0.23	–
0	0	–	20.1	–	3.2	–	0.68	–	0.17	–
4.8	5.9	5.7	18.5	19.6	3.0	3.2	0.64	0.68	0.13	0.14
10.0	12.0	11.1	18.3	20.6	2.8	3.1	0.67	0.75	0.16	0.18
20.0	24.0	22.3	15.3	19.7	2.4	3.1	0.51	0.66	0.13	0.17

[a] Gravimetrically determined.
[b] Values for matrix (calculated with M_{ox}).

TABLE III Composition by XRF of materials extruded with reduction ratio of 18:1

V_f (vol%)	M_f	Composition (wt%)							
		[Si]	[Si][a]	[Cu]	[Cu][a]	[Mg]	[Mg][a]	[Fe]	[Fe][a]
0	0	18.7	–	2.9	–	1.2	–	0.3	–
4.8	5.9	17.9	19.0	2.9	3.1	1.1	1.2	0.4	0.4
10.0	12.0	16.3	18.3	2.5	2.8	0.9	1.0	0.5	0.6
20.0	24.0	16.1	20.7	2.7	3.5	0.8	1.0	0.5	0.6

[a] Values for matrix (calculated with M_{ox})

3. Results

3.1. Chemical analysis

The results of the chemical analyses using the two methods are presented in Tables II and III. The magnesium and iron contents of the matrix alloy determined by ICP–OES are somewhat lower than expected. These may contain errors relating to the method of disclosing, because XRF gives values more in the nominal range (Table III). However, the composition of the extruded base alloy does correspond well with the composition of the base alloy powder, determined by the same method (Table II). Significant compositional changes in the matrix of the composites as a result of material preparation have not been observed.

The measured mass fractions, M_{ox} of oxide (fibre) material are systematically too low. This is not as expected, because the oxide fractions of the base alloy are included in these values. Therefore, we are aware of the possibility of some dissolution of the porous fibre during the analyses. The data are considered to be insufficiently reliable to oppose the nominal fibre loading values.

3.2. Densities

For the calculation of the relative densities of the composites, the density of the fibre ρ_f, is actually needed. Whilst the manufacturer states a value of 3.3 $\times 10^3\ kg\,m^{-3}$, this value is doubted at the present stage. We predict a value of $\rho_f = 3.0 \times 10^3\ kg\,m^{-3}$ (value corrected with respect to our last communication [11]) based on helium pycnometry and assessment of internal pore volume by nitrogen adsorption measurements

$$\rho_f = \left(\frac{1}{\rho_{true}} + V_P\right)^{-1} = \left(\frac{1}{3.52} + 0.045\right)^{-1} = 3.0 \times 10^3\ kg\,m^{-3} \quad (1)$$

where ρ_{true} is the true material density (measured by helium pycnometry [11]) and V_p the specific pore volume (measured by nitrogen adsorption [11]).

Absolute densities of the composite materials are given in Table IV. These values can provide some indication of the density difference between matrix and fibre. Indeed, densities of the composites are not very much higher than those of the base alloy suggesting that the difference in density with that of the fibre is small. With the exception of material with $V_f = 0.200$ extruded at an ER of 38:1, the applied reduction ratios of extrusion hardly have a significant

TABLE IV Absolute densities (experimental error $\pm$ 0.01) of composite materials as determined by weight measurement using Archimedes' principle

Nominal fibre volume fraction, V_f	Absolute density ($10^3\ kg\,m^{-3}$)		
	ER = 10:1	ER = 18:1	ER = 38:1
0	2.67	2.64	2.67
0.048	2.68	2.69	2.69
0.100	2.71	2.70	2.72
0.200	2.72	2.73	2.78

TABLE V Relative densities and actual fibre volume fraction $(V_f)_a$ of composite materials derived from M_f (Table III), the data of Table IV and a fibre density of 3.0×10^3 kg m^{-3}

V_f	$(V_f)_a$	Theor. density (10^3 kg m^{-3})	Relative density (% ± 0.5%)		
			ER = 10:1	ER = 18:1	ER = 38:1
0	–	2.67	100.0	98.9	100.0
0.048	0.052	2.69	99.6	100.0	100.0
0.100	0.108	2.71	100.0	99.6	100.4
0.200	0.214	2.75	98.9	99.3	101.1

TABLE VI Results of hydrogen analyses of the materials extruded at different extrusion ratios.

Nominal fibre volume fraction, V_f	Hydrogen content (p.p.m.)		
	ER = 10:1	ER = 18:1	ER = 38:1
0	⩽ 0.1	0.1 ± 0.1	0.1 ± 0.1
0.048	0.1 ± 0.1	0.2 ± 0.1	0.3 ± 0.1
0.100	0.1–7.8[a]	0.3 ± 0.2	1.2[a]–9.0[a]
0.200	2.2[a]–19.1[a]	0.7 ± 0.2	2.9[a]–14.1[a]

The error given for some materials is from three-fold measurements
[a]Refers to the presence of sub-signal of type B in the hydrogen time spectrum. Bar-separated values give the range of the data.

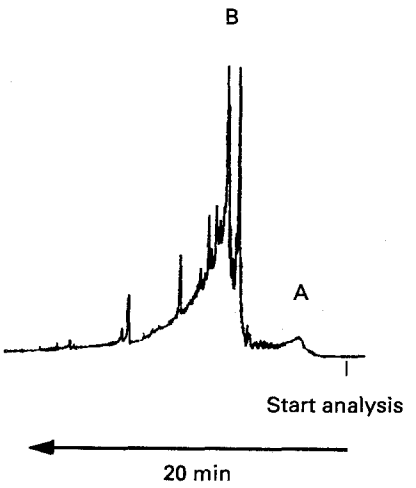

Figure 2 Typical hydrogen spectrum comprising sub-signals A and B. Time proceeding in direction of negative ordinate.

effect on density. Taking the nominal fibre mass fractions, M_f, as correct values and assuming a fibre density of 3.0, the relative densities in Table V are obtained. From these data it appears that except for the $V_f = 0.200$/ER 10:1 material, all composites are fully dense. The actual volume fractions $(V_f)_a$, calculated with a fibre density of $\rho_f = 3.0 \times 10^3$ kg m^{-3} are in excess of the nominal values (Table V).

3.3. Hydrogen content

The hydrogen contents of the materials after extrusion are given in Table VI. Substantial differences occur and a general trend is seen in a higher content with increasing fibre volume fraction. The corresponding hydrogen signals recorded against time at most display two distinctive parts. One such complete signal is shown in Fig. 2. The first part (A) with small contribution has a peak occurring after a constant time lapse of ~ 200 s of furnace residence. Part B comprises a more complex signal composed of a rapid increase in the hydrogen flux followed by a decay with superimposed spiky peaks. This part B was only observed for the materials with $V_f = 0.100$ and higher, extruded with extrusion ratios of 38:1 and 10:1. The presence of signal B gives rise to values of hydrogen content above 1 p.p.m.

3.4. Tensile properties

The ultimate tensile strengths (UTS) at room temperature are plotted in Fig. 3. In this and following graphs, the actual volume fractions, $(V_f)_a$ (Table V), are plotted while the text refers to the nominal volume

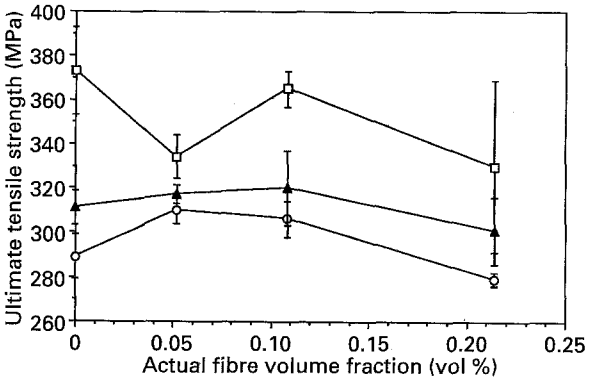

Figure 3 Ultimate tensile strengths of the materials at room temperature. ER: (○) 10:1, (▲) 18:1, (□) 38:1.

fractions, V_f. The data in Fig. 3 suggest that a higher reduction ratio gives rise to a higher average strength. Despite rather large standard errors, it may be argued that the composites extruded at ER = 38:1 with average strengths all lower than that of the base alloy, behave in the worst sense. Composites with volume fractions up to 0.100 extruded at ER 18:1 and 10:1, tend to show a small increase in average strength as compared to the base alloy extruded under the same conditions. Amongst the elongation data of the composites, no significant differences occur with extrusion reduction ratio (Fig. 4). However, a remarkably higher elongation value was found for the matrix alloy extruded at ER 38:1. Composites with $V_f = 0.200$ lag

behind with respect to both UTS and elongation values. These results are interpreted in terms of microstructural imperfections and will be treated in Section 4.

Fig. 5 presents the elastic moduli of the composites. Taking account of the large scatter, one may remark that the average values are increasing with decreasing reduction ratio, although in some cases the differences are insignificant. However, the differences in modulus between the materials (except for $V_f = 0.200$) extruded at ER 38:1 and the others, are obvious.

The behaviour of the composites with regard to the strength at 250 °C (Fig. 6) is very different from that at room temperature. Under this condition, all the composites are significantly stronger than the base alloy. The composites with $V_f = 0.048$ and 0.100 extruded with the highest reduction ratio are still strongest at 250 °C. The most regular increase in strength with increasing fibre volume fraction was observed for materials with ER = 18:1. Fig. 7 gives the plastic elongations of the materials, from which one can conclude that the better results at high volume fractions are obtained for an ER of 18:1.

For material extruded at ER = 18:1, the tensile strength was also determined at 350 °C. In Fig. 8 tensile strength data are presented collectively. Similar levels of relative strengthening occur at both elevated temperatures (Fig. 9).

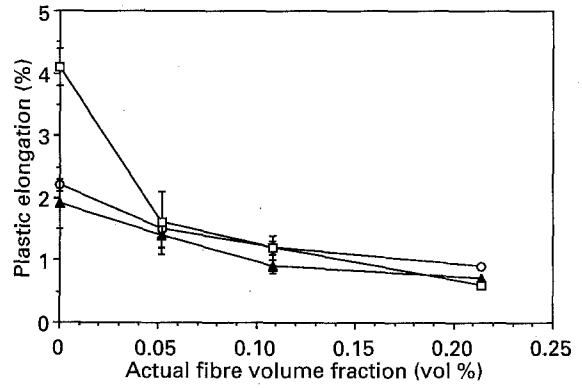

Figure 4 Permanent elongation data of the materials at room temperature. For key, see Fig. 3.

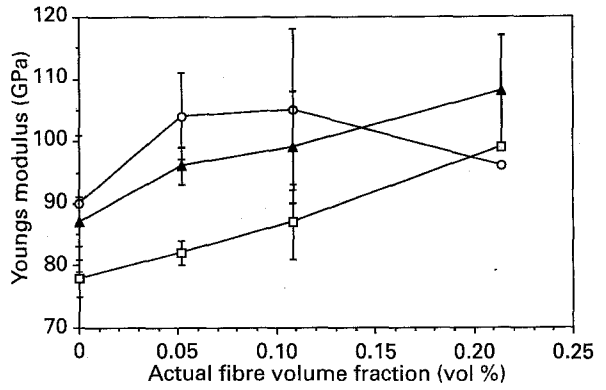

Figure 5 Elastic moduli in longitudinal direction of the materials at room temperature. For key, see Fig. 3.

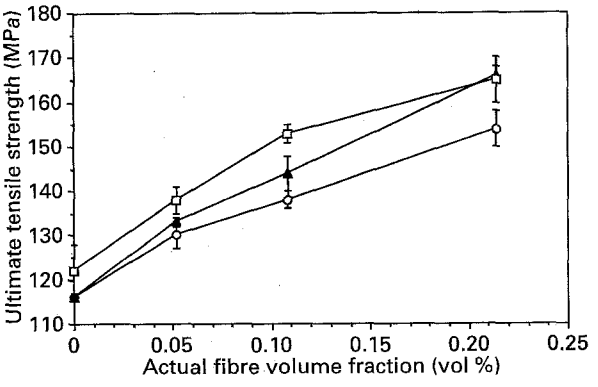

Figure 6 Ultimate tensile strengths of the materials at 250 °C. For key, see Fig. 3.

3.5. Microstructure and fibre length

3.5.1. Microstructure

Optical micrographs of the materials extruded at 18:1 are given in Figs 10–12. They were taken on as-polished surfaces. Note the variance in brightness of the fibres in longitudinal sections due to differing conditions of internal reflection. The distribution of fibres in transverse cross-sections is most uniform for fibre loadings of $V_f = 0.048$. In longitudinal sections of composites with $V_f = 0.100$ and 0.200, a banding of fibre-enriched and depleted layers is very pronounced.

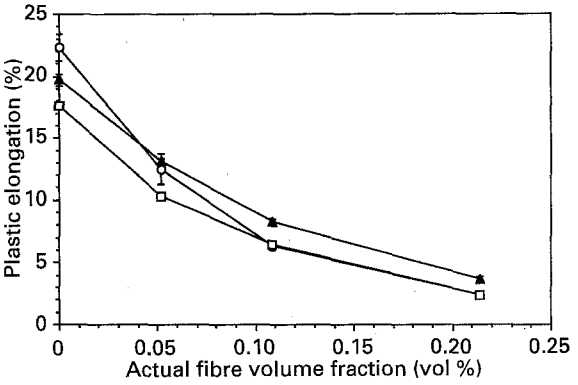

Figure 7 Permanent elongation data of the materials at 250 °C. For key, see Fig. 3.

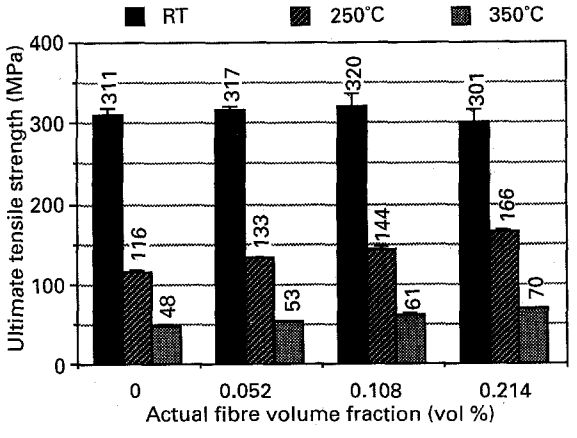

Figure 8 Bar diagram of ultimate tensile strength data of materials extruded at ER = 18:1.

Within these highly enriched layers, mainly in $V_f = 0.100$ and 0.200 composites, similarly elongated cavities are present. In transverse sections, their equivalents consist basically of regions of aggregated fibres with centrally positioned cavities. These fibre cluster regions can indeed be traced back to clusters present in the compacted powder billet, by sectioning of an incompletely extruded billet.

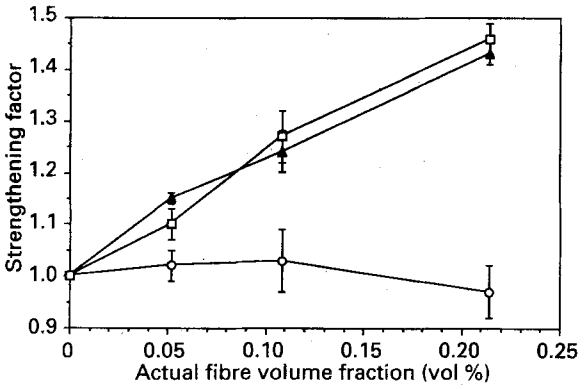

Figure 9 Relative strength increase of composites extruded at ER = 18:1. (○) RT, (▲) 250 °C, (□) 350 °C.

3.5.2. Fibre length in extruded materials

The micrographs in Figs 10–12 reveal that little remains of the initial length of the fibres. Table VII gives the fibre length distribution statistics obtained with Method A. The distributions of fibre length are characterized by the geometric mean, L_g, and standard deviation, σ_g. The use of these statistics was elucidated in an earlier publication [18]. No significant changes in mean fibre length occur among the three extrusion reduction ratios. Cumulative fibre length distributions

TABLE VII Results of fibre size analyses of the composites. Geometrical mean, L_g and standard deviation, σ_g are given

Nominal fibre Volume fraction V_f	ER 10:1		18:1		38:1	
	L_g(μm)	σ_g	L_g(μm)	σ_g	L_g(μm)	σ_g
0	–	–	–	–	–	–
0.048	9.4	1.76	9.2	1.80	9.3	1.74
0.100	7.8	1.67	8.0	1.64	8.1	1.60
0.200	6.4	1.49	6.5	1.51	6.3	1.49

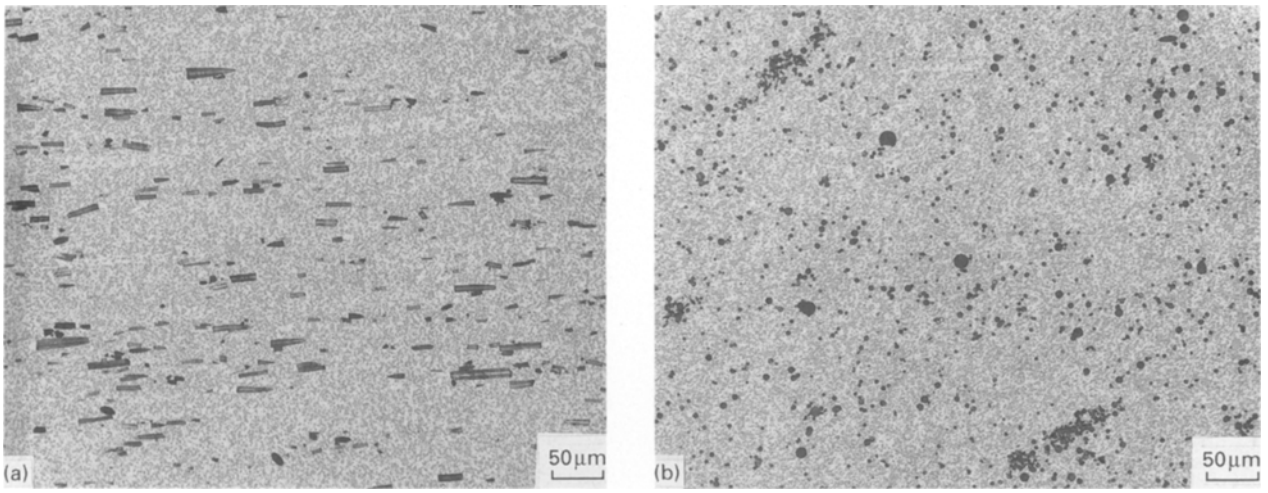

Figure 10 Optical micrographs of $V_f = 0.048$/ER = 18:1 composite in (a) longitudinal section, and (b) transverse section.

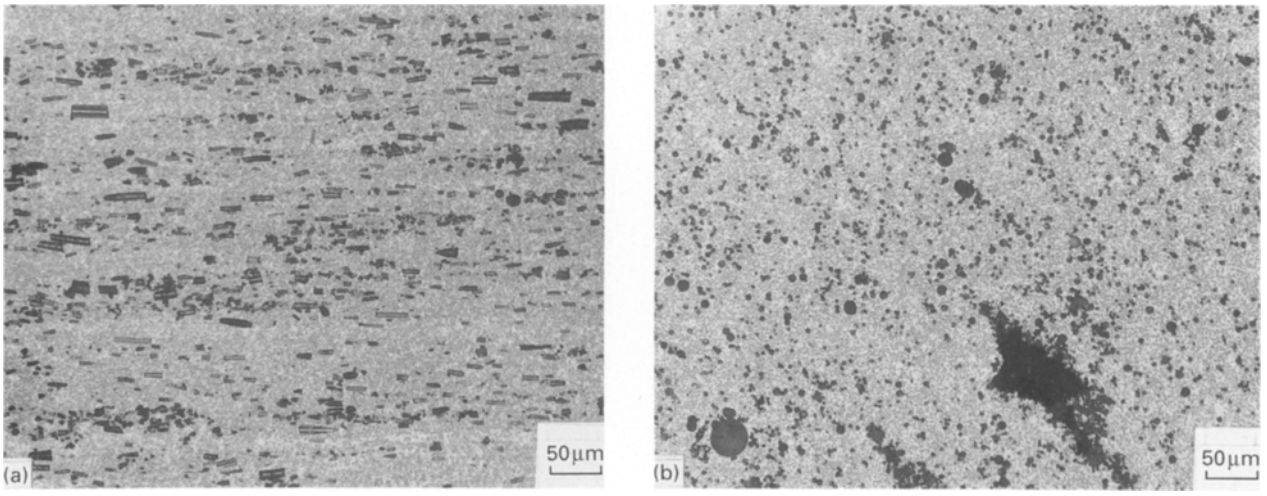

Figure 11 Optical micrographs of $V_f = 0.100$/ER = 18:1 composite in (a) longitudinal section, and (b) transverse section.

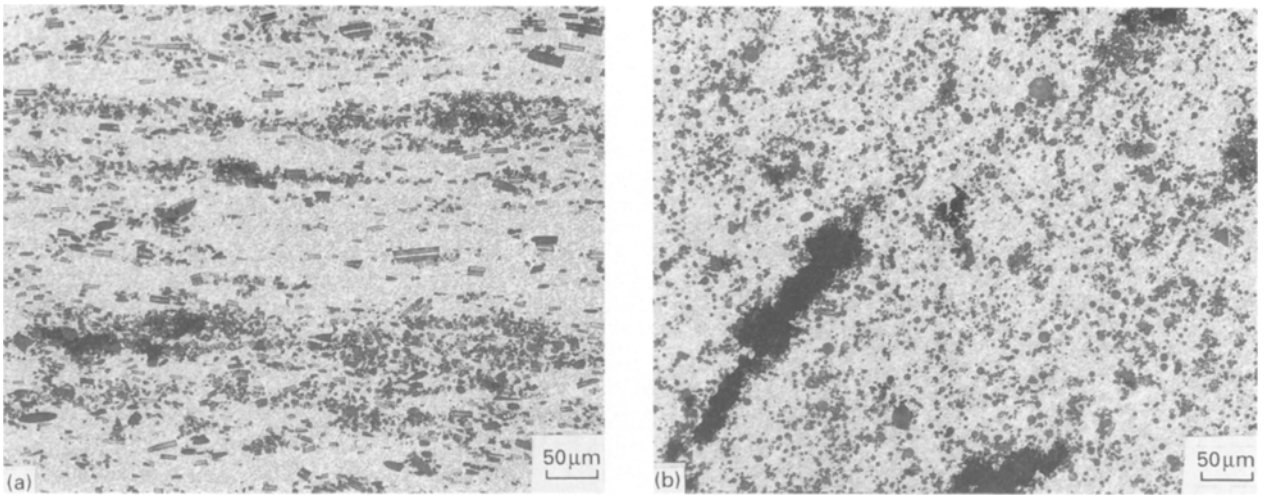

Figure 12 Optical micrographs of $V_f = 0.200$/ER = 18:1 composite (a) longitudinal section, and (b) transverse section.

of the composites extruded at ER = 18:1 are presented in Fig. 13. No fibre fragments were encountered with a size $L < 3.5$ μm. This can be understood by realizing that the software measures the largest dimension of a fibre fragment which, if only normal fracture occurs, will ultimately be the fibre diameter. It is noted that the distributions are not symmetrical on the log scale. Distributions of fibre length corresponding to the data in Table VII (measured on samples by Method A) do not pass the χ^2-test for log normality. Therefore, the added value of the geometrical mean and standard deviation in characterizing the fibre length distribution, has disappeared. However, we will not refrain from their use because they characterize the negatively skewed distribution better than do their arithmetical equivalents.

3.5.3. Fibre length after P/M processing stages

In Table VIII the lengths of fibres after each individual processing step are given. As expected, the largest reduction in fibre size was found to occur during the mixing. The fibre length distributions obtained at that stage all passed the test for log normality [18]. Precompaction led to additional breakage while the log normality characteristic of fibre length remained [19]. Extrusion again gave rise to extensive breakage, bringing down mean fibre size by a factor ~ 3. The cumulative distributions, some of which were presented above, do not show the characteristic point symmetric S-shape of the previous distributions, nor do they pass the test for log normality. However, it should be noted again that the fibre lengths in the extruded materials were measured alternatively (*in situ*) on metallographical sections (Method A).

TABLE VIII Fibre lengths during production

	L_g (μm) at nominal fibre volume fraction, V_f		
	0.048	0.100	0.200
As-received Saffil milled fibre length	← ≈ 200[a] →		
After mixing in ball-mill	38	30	25
After canned per-compaction	29	22	20
After full compaction/extrusion	9	8	6

[a] ICI, Runcorn, UK; non-specified average.

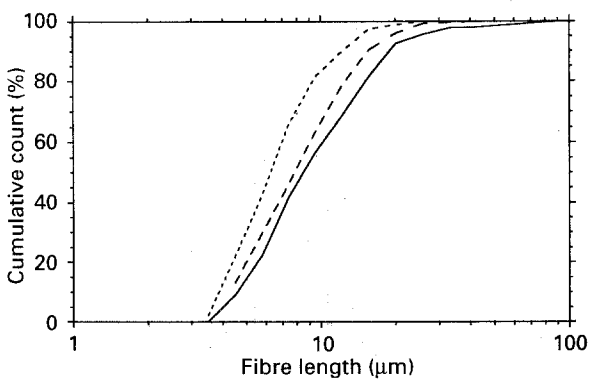

Figure 13 Cumulative fibre length distributions measured by Method A in composites extruded at ER = 18:1 V_f (vol%); (——) 0.048, (– – –) 0.100 (- - -) 0.200.

To check if the character of the fibre-size distributions had indeed changed after extrusion, fibres were also measured in a sample prepared by Method B of the composite with $V_f = 0.100$ and ER = 18:1. Fig. 14 presents and compares the results obtained with both methods. It appears that for this method B the results obtained are different. A higher geometrical mean, L_g (10.4 compared with 8.0), a lower geometrical standard deviation, σ_g (1.56 compared with 1.64) and an acceptance of the log normality hypothesis was found. The reason why the fibre length distributions obtained with Method A did not conform to log normality is most likely an imperfect alignment of these fibres. In that case, a lower, apparent size of a fraction of the fibres is measured, giving a positive bias to low sizes.

The deformation pattern during extrusion varies in space as well as time. Therefore, an attempt was made to determine at which stage of extrusion and location in the material the most intense fracture occurred.

3.5.4. Fibre length during extrusion

Extrusion of a porous metal powder compact involves a characteristic sequence of flow stages appearing in the pressure versus ram displacement curve (Fig. 15 [20]). The first, non-linear stage (A) corresponds to the compaction of the porous billet to near theoretical density. Subsequently, the pressure rapidly increases in a linear way until a peak value is reached. At a stage prior to attainment of the peak value, extrusion takes off. After the peak, pressure reduces to a steady state value (Stage C). For the present base alloy, the difference between peak pressure, (p_m), and steady state pressure, (p_s), is very large due to the high work-hardening capacity of the alloy. An extensive description of the extrusion pressure–displacement diagram of the base alloy is given elsewhere [20].

The length of fibres was studied in a billet partially extruded to a stage beyond the peak pressure (Stage B). Thus, the consolidation Stage A had been passed. The material was $V_f = 0.100$ composite at an ER of 18:1. Fibre lengths were measured in selected areas of interest (Fig. 16). By necessity, samples were prepared according to Method B because at this stage fibres are far from being aligned, and thus could not be measured in cross-section. Slices of ~ 1 mm thickness taken from the areas indicated were dissolved. The results are given in the map of Fig. 16. A large difference in mean length (of a factor 2) occurs, compared with that after pre-compaction (Table VIII), implying that most of the breakage occurs during the consolidation (Stage A) of extrusion. The size distributions all pass the test for log normality. Only small variations in mean size can be observed among samples from different locations, e.g. between the dead-metal zone and the area in front of the die-opening.

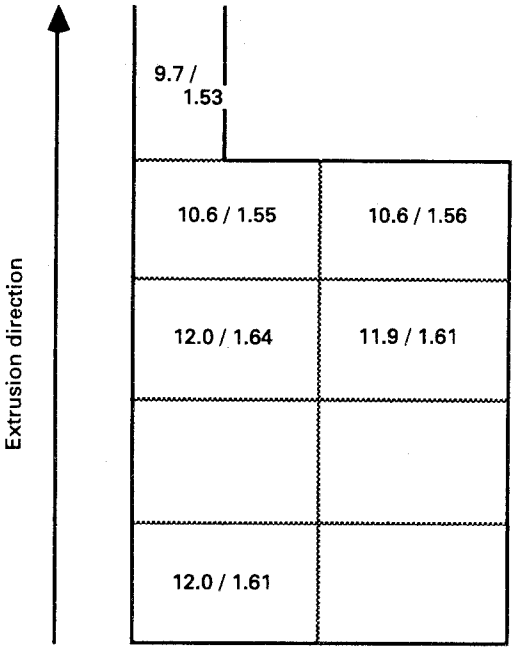

Figure 16 Map section through half of a partially extruded billet of a $V_f = 0.100$/ER = 18:1 composite, with values of geometric mean L_g (μm) and standard deviation σ_g (dimensionless) of fibre lengths.

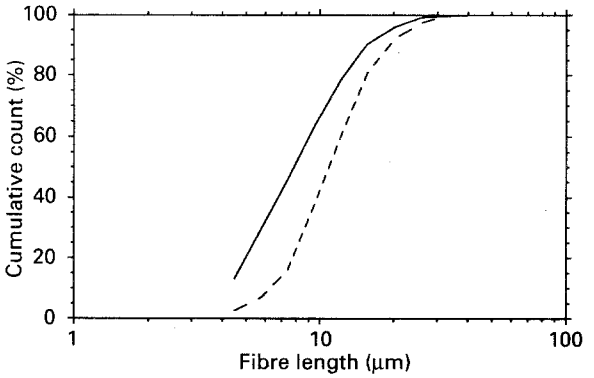

Figure 14 Cumulative fibre length distributions measured by Methods (——)A and (– – –)B in $V_f = 0.100$/ER = 18:1 composite.

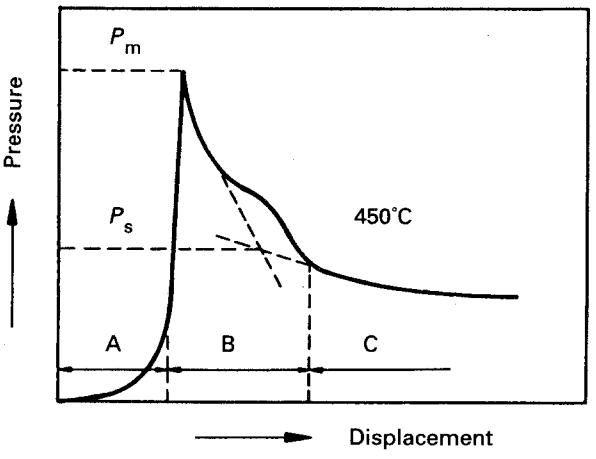

Figure 15 Typical ram displacement versus extrusion pressure curves for the present base alloy [20].

3.6. Fractography

On examination of the fracture surfaces of samples tested at room temperature and 250 °C by scanning electron microscopy (SEM), the following features were marked. Under both test conditions, cell-like depressions were highly characteristic. These dimple structures are representative of ductile void formation in the matrix. They are often related to the presence of (or centred at) fractured irregular particles, interpreted as silicon crystals. The dimple boundaries may also be centred around fibres, whose circular contours are often hardly distinguishable. Fibres do not usually stand out of the fracture surface (Fig. 17a). The fibre protruding slightly in the left part of this image is coated with a matrix phase appearing brittle. Because the fibre had also lost its circular cross-section, it is believed that decohesion had occurred along this cladding phase. Brittle intermetallics on the surface of alumina fibre were indeed shown to be capable of influencing the fracture morphology of fibres in a composite [21]. When fibres are gathered in an aggregate, decohesion at the fibre–matrix interface may be observed (Fig. 17b). Thus, pull-out is not widespread, indicating that a good bond exists between matrix and fibre, except for the aggregated fibre regions.

Because it is very difficult to recognize a fibre in the SEM image, it is nearly impossible to make conclusive

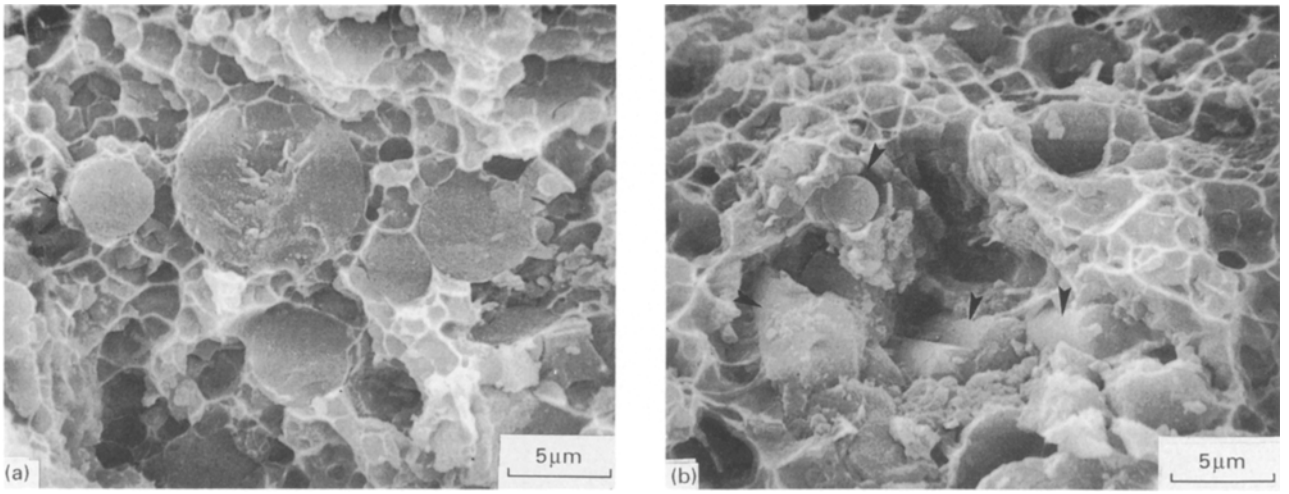

Figure 17 SEM microfractrographs of $V_f = 0.100$/ER = 18:1 material showing (a) well-bonded fibres (test at room temperature) and (b) closely packed fibres with a lack of bonding (arrows).

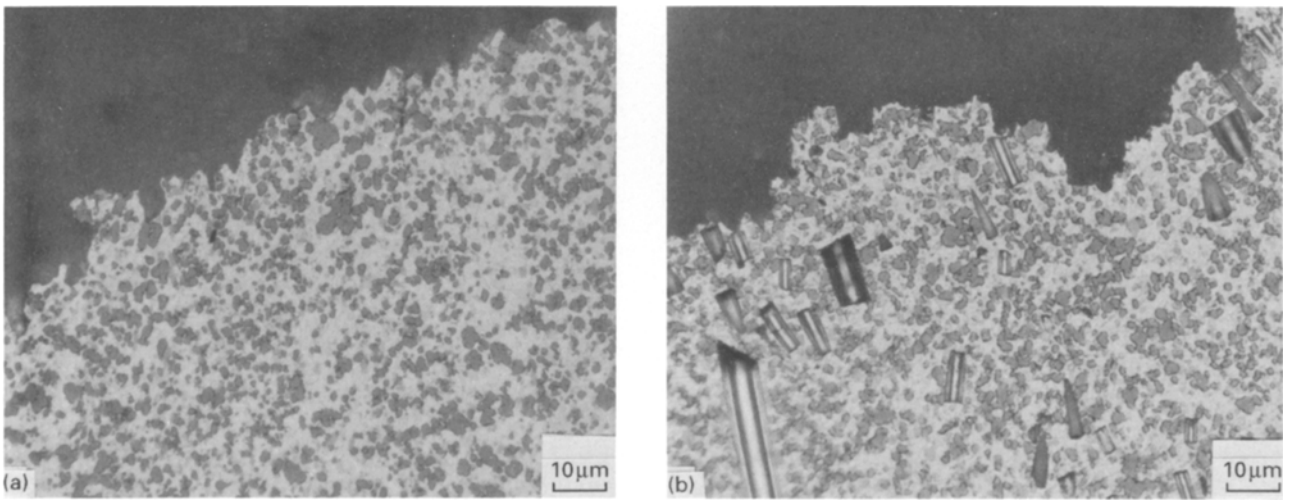

Figure 18 Optical micrographs of longitudinal sections through the fracture surface of samples of (a) $V_f = 0$, and (b) $V_f = 0.100$ materials with ER = 18:1, tested at 250 °C.

statements on differences in fracture appearances between different materials and test conditions, let alone on differences in fracture mechanisms.

Fig. 18 shows optical micrographs of the $V_f = 0$ and 0.100/ER = 18:1 materials tested at 250 °C which suggest that the fracture path is determined to a large extent by the (presence of) silicon particles. Fibres in the vicinity of the fracture surface can be seen to have nucleated voids only at their terminations, although mostly a fraction of these fibre ends remains covered with metal. This feature, again emphasizing the good bond between matrix and fibre, is clear from the microfractograph of Fig. 19.

4. Discussion

4.1. Microstructure

All composites at all reduction ratios of extrusion (higher V_f materials to a larger extent) do show elongated cavities related to stringers of fibres. It is believed that the cavities arise from decohesion and expellation of (mostly) fibre material during cutting and grinding operations. Support for this viewpoint is given by the density data for $V_f = 0.100$ revealing no porosity. Apparently, the plastic strain in and around these clustered fibre regions was insufficient to obtain a good internal bonding. This deformation shielding

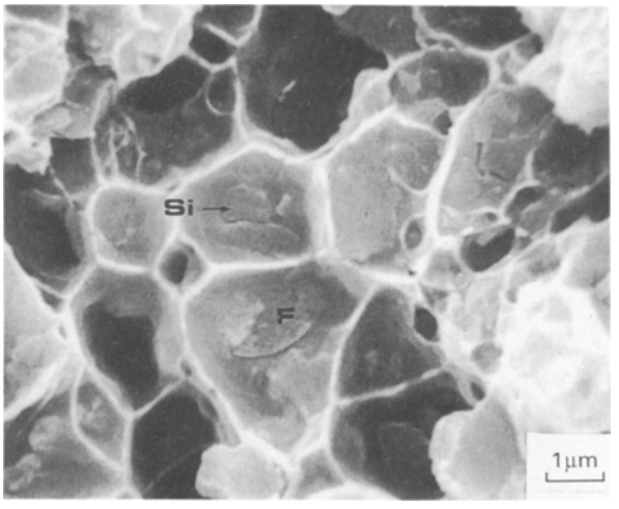

Figure 19 SEM microfractographs of $V_f = 0.100$/ER = 38:1 material (test at 250 °C) showing voids nucleating at the fibre interface with matrix and a silicon particle, leaving matrix metal adhering to the fibre end (F).

effect of relatively hard regions of concentrated ceramic phase was also encountered by other workers [22, 23] and may be identified as a major problem in the deformation consolidation processing of P/M metal matrix composites (MMCs). It may only be solved by taking even more care in preparing and maintaining homogeneous powder mixtures.

4.2. Fibre length

No significant changes in mean fibre length occurred with varying extrusion reduction ratio. It was also concluded that the largest size reduction during extrusion takes place in the initial consolidation stage (Stage A, Fig. 15). Both results are in accordance for the following reason. The maximum pressure during the compaction stage of extrusion for one and the same material is not likely to change with reduction ratio, because compaction occurs before the actual extrusion and attainment of peak pressure. Thus, fibre breakage at this stage will be similar for a single material at various extrusion ratios. After the compaction stage, the shearing part of extrusion takes place, with high shear strain rates. With respect to fibre breakage in this stage, the various reduction ratios applied apparently did not involve large variations.

How is this possible? It is likely that many fibres fracture in a bending–loading mode during rotation in the plastically consolidating matrix. Initially, fibres are oriented in all directions. During compaction in Stage A, they tend to orient normal to the applied extrusion force. Afterwards, progressive reorientation occurs towards the shear planes of extrusion. In both these stages of reorientation, bending may take place due to inhomogeneous flow of matrix surrounding the fibre. It will be clear that these flow inhomogeneities, responsible for bending forces, can be largest in the compaction stage when porosity exists. Consideration of the force on a fibre during bending may provide some insight in fibre fragmentation during these stages of extrusion. The relation for the minimum bend radius, λ_{min}, at which fracture occurs, is

$$\lambda_{min} = \frac{E_f d_f}{2\sigma_{uf}} \quad (2)$$

Where E_f is the fibres Young's modulus and d_f its diameter. Substituting Equation 2 in the equation for the bending moment

$$M = \frac{\pi d_f^4 E_f}{64\lambda} \quad (3)$$

and putting $M = CFL$ (in which C is a constant) we find the following dependence of the (maximum) bending force at fracture on fibre length

$$(F)_{\text{at fracture}} \sim \frac{1}{L_f} \quad (4)$$

It appears that the bending force for breakage drastically increases with decreasing fibre length. With lowering fibre size, further breakage becomes progressively more difficult. Moreover, the flow pattern in the high shearing part of extrusion will be more homogeneous, allowing more fibres to rotate as rigid bodies without large bending forces.

4.3. Hydrogen levels

In the analysis of hydrogen, it was found that the presence of Signal B gives rise to values of hydrogen content above 1 p.p.m. The shape of the hydrogen signal is interpreted as follows. Taking the diffusion coefficient of hydrogen in pure solid aluminium from Eichenauer and Pebler [24], a diffusion distance, $x = (Dt)^{1/2}$ of 0.23×10^{-2} m is calculated for the peak time (200 s) of Signal A, which corresponds to nearly half the sample diameter. Therefore, signal A could have arisen from volume diffusion of hydrogen through the whole sample section. If any diffusion of hydrogen representing signal A occurred along grain boundaries, it obviously did not do so at higher rates than during (volume) diffusion in cast pure aluminium. Furthermore, it suggests that Signal B represents (molecular) hydrogen which had piled up internally before escaping massively. Such high hydrogen levels after degassing are unlikely to arise from residual moisture at the prior particle boundaries (PPBs). They are, therefore, most likely caused by residual water of the fibres (see also [11]).

During preheating and extrusion (at 450 °C) of the pre-compacted billets, any residual water in the fibres may be liberated and react with the aluminium powder particles to form hydrogen. The hydrogen will be partly stored in the extruded aluminium. The differences in hydrogen content among the materials at different extrusion ratios are hard to explain. There are several possible options. Firstly, excessive fibre damage during extrusion in the form of microcracks may expose the internal surface of the fibre so that internally residing water may rapidly evolve as hydrogen. Cracks in fibres were most frequently observed in high V_f materials extruded at 38:1. Low values of hydrogen may, therefore, be related to low rates of hydrogen evolution. Secondly, differences may exist in numbers of physical traps for (molecular) hydrogen during and after extrusion. Such traps could consist of dislocations, grain boundaries, PPBs, voids, pores, etc., and may thus introduce a dependence of hydrogen content on (extrusion) processing. Whereas too high an extrusion ratio will cause excess deformation and creation of sessile dislocation networks, grain refinement and a consequently high hydrogen trapping potential, a low extrusion ratio may also be responsible for high amounts of trapped hydrogen by its collection in pores. The presence of some porosity may indeed be inferred for $V_f = 0.200$ material extruded at 10:1 (Table V). A third explanation of the observed differences involves the state of degassing. It is possible that during storage, some of the degassed powders experienced renewed uptake of moisture from the atmosphere (by oppression of the argon) through small holes in the weldings of the can. However, the observed preference for high and low values of hydrogen makes such a probabilistic explanation unlikely. A complicating effect which could have played a role is that degassing of the high V_f materials

was insufficient: a single set of parameters was used for all composites.

4.4. Mechanical properties

The moduli of the materials (except for $V_f = 0.200$) extruded at ER = 38:1 are definitely lower than those of the others. It was previously proposed by Zhou and Duszczyk [8] that decohesion of the interface of silicon and aluminium may occur in the base alloy as a result of the high strain rate involved in extrusion with a (too) high reduction ratio. Therefore, the low moduli of the materials could well arise from reduced stress transfer from matrix to silicon particles.

A significantly higher strength was found for the composites extruded at 38:1, compared to those at lower reduction ratios. It is noted that the strength of the base alloy also significantly increases with increasing reduction ratio. The plastic elongation of the base alloy extruded at 38:1 was twice as high as of those extruded at lower extrusion ratios. This strongly suggests an effect of matrix microstructure. It is obvious that the matrix in the case of the 38:1 materials is strained to the highest extent during extrusion. A consequently high dislocation density and fine substructure after recrystallization may give rise to a higher rate of work hardening and a higher flow stress.

Thus, at room temperature these composites may be regarded as having matrices with flow stress differing for each of the applied extrusion ratios. One should also be aware of variations in matrix straining and thus microstructural development during extrusion among materials (at one extrusion ratio) with different V_f. This is a result of the total matrix strain during extrusion being equal to the macroscopic strain divided by the matrix volume fraction $(1 - V_f)$.

4.4.1. The effect of matrix strength on composite strengthening

The pattern of strength of the composites at room temperature relative to that of the base alloys is different for each of the three reduction ratios. At ER = 10:1, the $V_f = 0.048$, composite strength is higher while decreasing to the same level as the matrix for $V_f = 0.200$. At ER = 18:1, all the composites exhibit similar strength levels while at 38:1, a loss in strength for the $V_f = 0.048$ composite is followed by a return to the strength for the $V_f = 0.10$ composite to the level of the base alloy. Thus, an increase in strength of the base alloy with increasing extrusion ratio, has a negative effect on strengthening at room temperature.

This is apparently in line with a report of the conditions for strengthening as given by Friend [25], in which the strength of a discontinuous fibre-reinforced composite was predicted by a simple shear lag model. It was shown that a composite with a matrix, exhibiting a large difference between failure stress and yield stress (i.e. a high work-hardening material), would have less strengthening potential at low fibre volume fractions than a composite with a low work-hardening matrix. However, this report was based on the assumption that fibres were long enough for breakage at the fibre failure stress through transfer of load by shear. The critical fibre length above which this occurs is given by

$$L_c = \frac{\sigma_{uf} d_f}{2\tau} \tag{5}$$

where σ_{uf} is the fibre fracture strength, d_f the fibre diameter and τ the shear stress at the interface between matrix and fibre. One problem in calculating this parameter for the present combination of materials is the uncertainty in the value of τ. The base alloy work-hardens at a high rate and the yield point is not clearly defined. This is due to the presence of a dispersion of fine silicon particles, which give rise to stress concentrations and diffuse yielding. Nevertheless, an estimate from the room temperature stress–strain curves of samples of $V_f = 0$/ER = 38:1 amounts to $\sigma_y = 120$ MPa. By assuming $\tau = 1/2\ \sigma_y$ we obtain a value of L_c of

$$L_c = \frac{2000.3}{2.60} = 50\ \mu\text{m} \tag{6}$$

It is noted that during deformation. L_c might decrease somewhat due to an increase in τ by matrix hardening. If, in the present composites, L_c remains of the order of magnitude as given by Equation 6, shear-load transfer up to the fibre fracture stress is not likely to occur at room temperature in any of the composites.

Under the high-temperature conditions of testing, the strength and work hardening of the base alloy and matrix are lower than at room temperature. Because L_c will even be higher at elevated temperature than at room temperature (τ will decrease with increasing temperature), the observed strengthening at high temperature apparently conflicts with models of load transfer by shear.

4.4.2. Other strengthening effects in base alloy and composites

The metal matrix contains nearly 20 vol% silicon particles with sizes in the range 0.5–5 μm, as well as precipitates of several intermetallic (IM) phases [26]. When correct processing has kept these particles and their spacing fine enough, some small contribution to the room-temperature strength of dispersion hardening may be expected. Under the present elevated temperature test conditions, the strength of the base alloy has fallen drastically. After 100 h annealing, the dispersion hardening of silicon particles and intermetallic particles will most certainly have disappeared, due to coarsening. The main drop in strength will be caused by recovery of the deformation substructure in the aluminium matrix under the annealing conditions.

On cooling from the extrusion temperature, thermal residual stresses develop in the matrix around silicon (and IM) particles and fibres due to mismatching coefficients of thermal expansion, CTEs. These stresses may be relieved by the punching of prismatic dislocation loops [27], consequently increasing the

dislocation density. The interaction of mobile dislocations with the aforementioned and the residual stresses is responsible for a significant strengthening effect in MMCs. Arsenault and Shi [27] derived an expression to predict the dislocation density in the matrix of an equiaxed particulate-reinforced MMC after complete relaxation of the CTE misfit

$$\bar{\rho} = \frac{A V_f e_T}{b(1 - V_f)} \frac{1}{t} \quad (7)$$

where e_T is the CTE misfit strain defined as $e_T = \Delta\alpha\Delta T$, t is the smallest dimension of a particulate, b is the Burgers vector and A is a geometrical factor, being 12 for equiaxed particles and 10 for short fibres of aspect ratio 2. Once $\bar{\rho}$ is calculated, the increase in flow stress, $\Delta\sigma_{CTE}$, may be estimated from

$$\Delta\sigma_{CTE} = \gamma G b \bar{\rho}^{1/2} \quad (8)$$

where γ is a constant of the order of 1, and G is the shear modulus of the aluminium matrix. Using the following material constants: $G = 26$ GPa [28], $b = 0.286$ nm [27], $\alpha_{[Al]}$ (at 25 °C) $= 22 \times 10^{-6}$ °C^{-1} [26], $\alpha_{[Si]} = 3 \times 10^{-6}$ °C^{-1} [29], $\alpha_{[Saffil]} = 8 \times 10^{-6}$ °C^{-1} [30], $t_{[Si]} = 2$ μm and $t_{[Al_2O_3]} = 3$ μm, the contributions to the flow strength of the alloys (after cooling from the extrusion temperature) due to this effect of silicon particles and fibres can be estimated (Table IX). It is remarkable to find a large share due to silicon particles. On top of that, the contribution issued by the presence of fibres is significant. The mechanism may partly be responsible for the observed room-temperature strength retention (or small increase) of the materials with low V_f extruded at 10:1 and 18:1 (Fig. 3). The model assumes that the work hardening of the matrix of the composite is the same as that of the base alloy. This is surely an oversimplification, because dislocations will interact with the ceramic phase and its residual stress field. The alignment of fibres may enhance this interaction.

In a review article on various models for the strengthening of MMCs with discontinuous reinforcement, Taya [31] concluded that their major strengthening is by these punched dislocations and a back-stress created around the particles during thermal processing due to mismatching CTEs. Taking notice of the behaviour of the present composites, this view is shared.

TABLE IX Contributions to the strength of materials by dislocation punching due to differences in CTE between metal matrix on one side and silicon and alumina fibre on the other side

	V_f (vol%)			
	0	0.048	0.100	0.200
Strength of material (MPa)	311	317	320	301
Contribution of:	silicon particles	Fibres	Fibres	Fibres
To flow stress of material (MPa)	47	14	21	31

The fact that the (relative) strengthening of the fibres at elevated temperature is so much higher than at room temperature may thus be explained by a combination of the following factors; (1) the loss of strengthening effects at elevated temperature due solely to characteristics of the base alloy, thus allowing for any fibre strengthening effect to be of significant magnitude; (2) the prevalence of a mechanism of strengthening based on the build up of stresses around fibres in the plastically flowing matrix [31], including those remaining from thermal processing; and (3) the low strain to failure at room temperature of the base alloy preventing a larger strengthening contribution of the fibres at room temperature by the mechanism under point 2.

5. Conclusions

1. Saffil short fibre-reinforced aluminium composites prepared along a P/M route were, from a viewpoint of the tensile mechanical properties in the longitudinal direction, best extruded at the intermediate extrusion reduction ratio 18:1 of the three investigated. A higher reduction ratio decreased the elastic modulus, most likely due to decohesion of silicon particles in the matrix while at the same time reducing the relative strengthening. A lower reduction ratio causes residual porosity at higher volume fractions.

2. Mean fibre length does not significantly change with reduction of the extrusion ratio. It was noticed that during extrusion, the most severe fibre breakage occurs in the initial compaction stage. Differences in fibre size and size distribution measured on samples of the same material prepared by two methods implied that fibre alignment in the extruded material was not perfect.

3. Large quantities of residual hydrogen, evolving during hydrogen analysis at 550 °C, were measured in $V_f = 0.100$ and 0.200 composites extruded at the highest and lowest reduction ratios. Some suggestions are given for explanation of these data. A relation between hydrogen levels and mechanical properties could not be established.

4. At 250 and 350 °C and prior annealing time of 100 h, the strengths of the composites in the longitudinal direction are significantly higher than those of the base alloy. For composites extruded at 18:1, the improvements were 15%, 24% and 43% at 250 °C for $V_f = 0.048$, 0.100, 0.200, respectively. Similar levels of relative strengthening occurred at 350 °C.

5. The combination of a shear lag model and the concept of a decreasing shear strength at the interface with increase in temperature, cannot account for the relative strength improvement at these conditions. It is suggested that strengthening is possible by the combined effect of a high ductility of the matrix and the resistance to plastic flow exerted by dislocations and stress fields around aligned fibres.

6. All of the composites processed contain fibre-enriched layers, having a bad internal coherance. They can be traced back as fibre clusters in the compacted powder. In fibre-rich layers, elongated cavities may form during machining and grinding operations. The

tensile properties in the transverse direction are therefore expected to be poor.

Acknowledgements

The authors acknowledge the support from and discussions with Professor B. M. Korevaar and the practical assistance of Wim Schuyt, and are grateful for the financial support of the Foundation for Technological Research (STW) and the Foundation for Fundamental Research of Matter (FOM).

References

1. T. W. CLYNE and J. F. MASON, *Metall. Trans.* **18A** (1987) 1519.
2. T. W. CLYNE, M. G. BADER, G. R. CAPPLEMAN and P. A. HUBERT, *J. Mater. Sci.* **20** (1985) 85.
3. A. SAKAMOTO, H. HASEGAWA and Y. MINODA, in "Proceedings of ICCM V," San Diego, California, July 1985.
4. K. SUGANUMA, T. OKAMOTO and N. SUZUKI, *J. Mater. Sci. Lett.* **6** (1987) 1347.
5. C. A. STANFORD-BEALE and T. W. CLYNE, *Comp. Sci. Technol.* **35** (1989), 121.
6. M. MACLEAN and R. DOWER, in "Proceedings of PM'90," London, UK, July 1990 (The Institute of Metals) p. 251.
7. J. L. ESTRADA HAEN, PhD thesis, Delft University of Technology (1990).
8. J. ZHOU and J. DUSZCZYK, *J. Mater. Sci.* **25** (1990) 4541.
9. *idem, ibid.* **26** (1991) 3737.
10. Saffil Datasheet, ICI Runcorn, UK.
11. J. H. TER HAAR and J. DUSZCZYK, *J. Mater. Sci.* in press.
12. *idem, Mater. Sci.Eng.* **A135** (1991) 65.
13. M. ICHIMURA, Y. SASAJIMA and M. IMABAYASHI, *Mater. Trans. JIM* **32** (1991) 1109.
14. *idem, ibid.* **33** (1992) 449.
15. W. THOMICH, *Stahl Eisen* **103** (1983) 497.
16. J. H. TER HAAR and J. DUSZCZYK, in preparation.
17. T. ALLEN, "Particle size Measurement", 3rd Edn, Powder Technology Series, (Chapman and Hall, London, 1981) p. 188.
18. J. H. TER HAAR and J. DUSZCZYK, *J. Mater. Sci.* **26** (1991) 3628.
19. *idem. ibid.* **27** (1992) 6495.
20. J. ZHOU and J. DUSZCZYK, *J. Mater. Shaping Technol.* **6** (1989) 241.
21. S. OCHIAI, T. ARAIKE, K. TOKINORI, K. OSAMURA, M. NAKATANI and K. YAMATSUTA, *J. Mater. Sci.* **27** (1992) 4667.
22. N. RAGHUNATHAN, H. B. MCSHANE, C. DAVIES and T. SHEPPARD, *ibid.* **25** (1990) 4906.
23. M. H. CARVALHO, T. MARCELO, H. CARCALHINHOS and C. M. CELLARS, *ibid.* **27** (1992) 2101.
24. W. EICHENAUER and A. PEBLER, *Z. Metallkde* **48** (1957) 373.
25. C. M. FRIEND, *J. Mater. Sci.* **22** (1987) 3005.
26. M. J. STARINK, V. JOORIS and P. VAN MOURIK, in "proceedings of the 12th RISØ International Symposium", Roskilde, Denmark, September 1991, edited by N. Hansen *et al.*, p. 675.
27. R. J. ARSENAULT and N. SHI, *Mater. Sci. Eng.* **81** (1986), 175.
28. B. DERBY and J. R. WALKER, *Scripta Metall.* **22** (1988), 529.
29. "CRC Handbook of Chemistry and Physics," 56th Edn (1975–1976) CRC Press, Boca Raton.
30. A. T. COLE, "Lecture Notes International Summerschool on MMCs," E-MRS May 1990, Klingenthal, France.
31. M. TAYA, *Mater. Trans JIM* **32** (1991) 1.

Received 12 January
and accepted 26 August 1993